

Results from SIM's Thermo-Opto-Mechanical (TOM3) Testbed

R. Goullioud*, C. A. Lindensmith, I. Hahn,

Jet Propulsion Laboratory, California Institute of Technology, 4800 Oak Grove Dr, Pasadena, CA 91109

ABSTRACT

Future space-based optical interferometers, such as the Space Interferometer Mission Planet Quest (SIM), require thermal stability of the optical wavefront to the level of picometers in order to produce astrometric data at the micro-arc-second level. In SIM, the internal path of the interferometer will be measured with a small metrology beam whereas the starlight fringe position is estimated from a large concentric annular beam. To achieve the micro-arc-second observation goal for SIM, it is necessary to maintain the optical path difference between the central and the outer annulus portions of the wavefront of the front-end telescope optics to a few tens of picometers.

The Thermo-Opto-Mechanical testbed (TOM3) was developed at the Jet Propulsion Laboratory to measure thermally induced optical deformations of a full-size flight-like beam compressor and siderostat, the two largest optics on SIM, in flight-like thermal environments. A Common Path Heterodyne Interferometer (COPHI) developed at JPL was used for the fine optical path difference measurement as the metrology sensor. The system was integrated inside a large vacuum chamber in order to mitigate the atmospheric and thermal disturbances. The siderostat was installed in a temperature-controlled thermal shroud inside the vacuum chamber, creating a flight-like thermal environment. Detailed thermal and structural models of the test articles (siderostat and compressor) were also developed for model prediction and correlation of the thermal deformations. Experimental data shows SIM required thermal stability of the test articles and good agreement with the model predictions.

Keywords: interferometry, metrology, wavefront, thermal, model, SIM.

1. INTRODUCTION

The TOM3 experiment is a key ground-based testbed that demonstrates critical technologies for SIM Planet Quest, a space-based Michelson interferometer that will carry out astrometry to micro-arcsecond precision on the visible light from a large sample of stars in our galaxy. Detail discussion regarding SIM is addressed by Marr¹.

SIM had many technological challenges to address in order to show the mission is technically achievable. These challenges range from nanometer-level control problems to picometer-level sensing problems². Several testbeds have been designed, built, and tested thus far in SIM's evolution. Each testbed is intended to resolve a system-level aspect of the SIM technology challenge. Examples of such testbeds include the SIM System Test-Bed 3³, Micro-Arcsecond Metrology testbed^{4,5}, and the Kite testbed⁶. The results from these series of testbeds form the evidence that the technological challenges faced by SIM are achievable.

Interferometry of such high precision requires extremely accurate knowledge of optical path length difference (OPD) changes, hence precise internal metrology, which is to be carried out with laser heterodyne metrology gauges. For SIM to succeed, the optical path length metric provided by the interferometer fringe determination must be consistent, at the level of tens of picometers, with the distances measured by metrology gauges, under the flight-like thermal environment. The purpose of TOM3 testbed is to demonstrate this agreement in a full-scale simulation that implements the front-end fraction of the final SIM flight functionality.

Figure 1 is a picture of the TOM3 hardware in the chamber that provides the vacuum necessary to obtain the required sub-nanometer stability. Figure 2 shows a schematic optical layout of the TOM3 experiment. TOM3 consists of the following major assemblies:

- The Common-Path Heterodyne Interferometer (COPHI) is the main optical sensor, designed to measure changes in the optical wavefront phase over the pupil after reflection on the test articles.
- The flight-like optical beam compressor assembly, described in more details in section 3, is the first test-article in this experiment. The compressor is used backward to expand the 50mm diameter COPHI metrology beam up to 350 mm in order to map the siderostat aperture.

* Email: renaud@jpl.nasa.gov; Phone: 818 354 7908

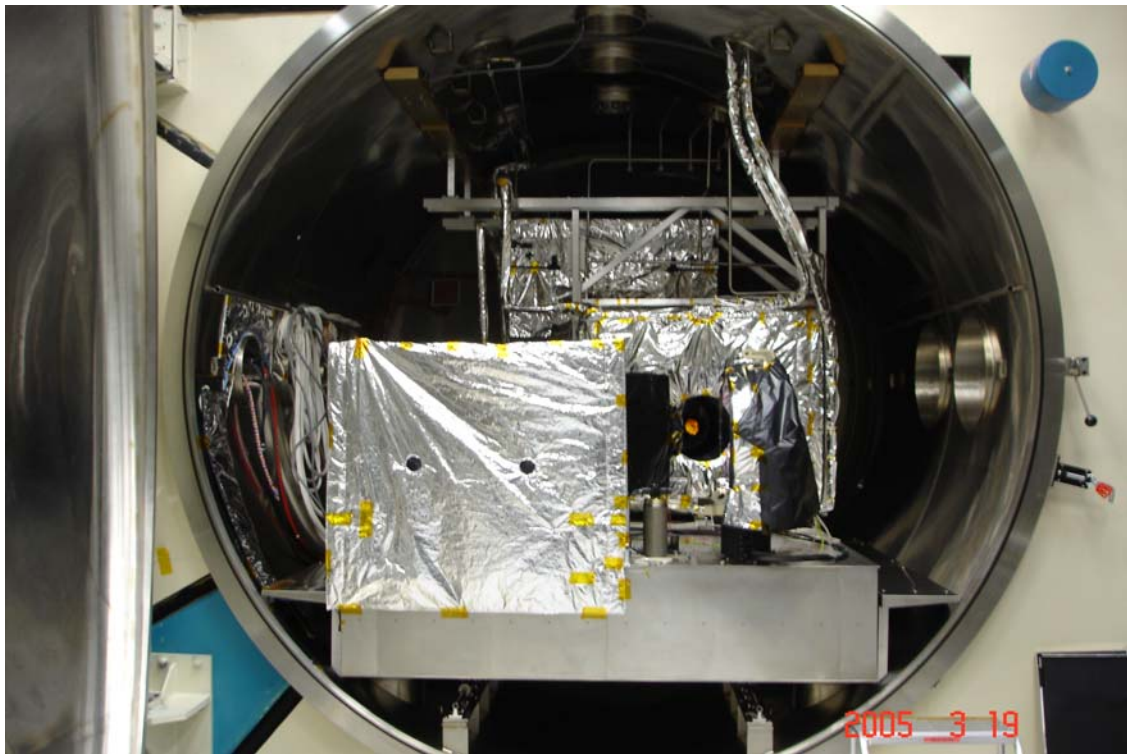


Figure 1. The TOM3 testbed in the 3.3 meter vacuum chamber at JPL.

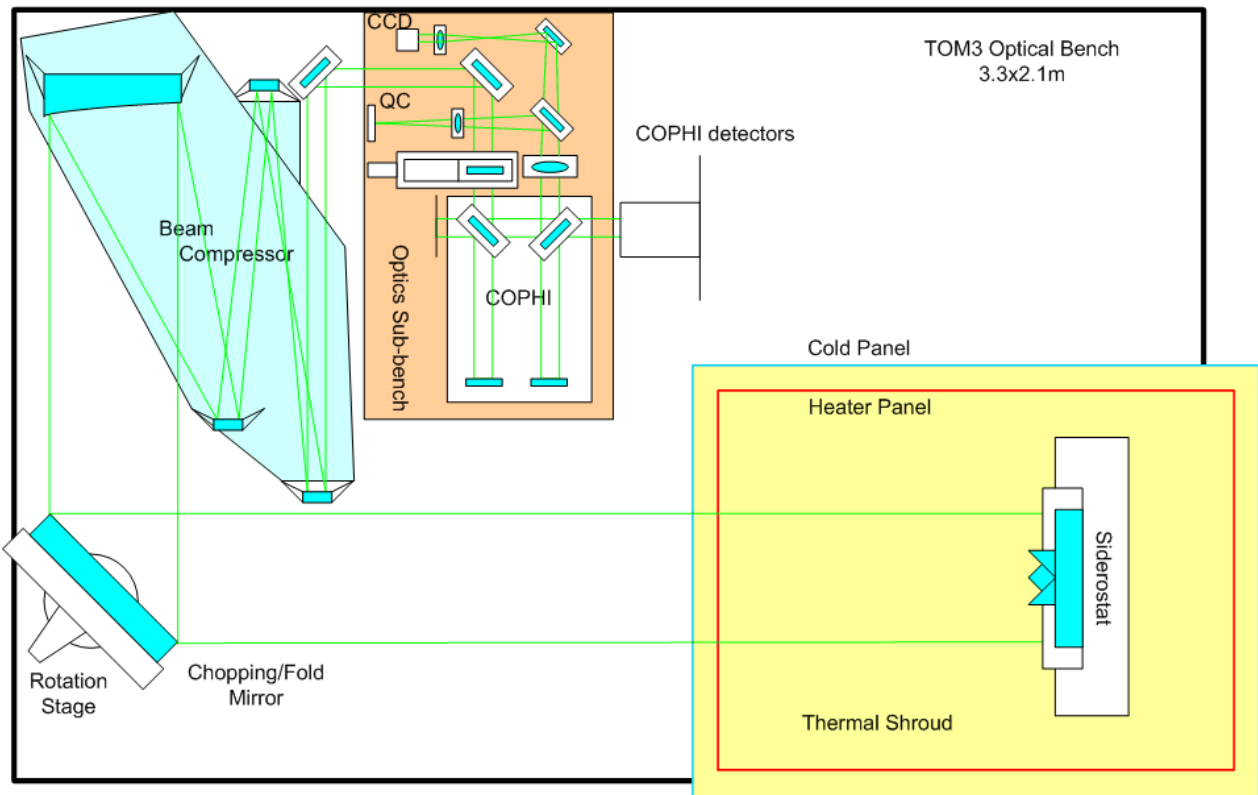


Figure 2. TOM3 main optical layout inside the vacuum chamber

- The chopping/fold mirror is a 500mm flat optic mounted on top of a motorized rotation stage that toggles between two positions. In the retro-mode position, the mirror is used as a reference while assessing the thermo-mechanical

performance of the beam compressor. In the siderostat mode, it is used as a fold mirror that relays the expanded COPHI beam out of the compressor onto the siderostat.

- The siderostat is SIM's starlight collecting aperture of the science interferometer. In the TOM3 experiment, it is the main test-article that retro-reflects the metrology beam back to the COPHI sensor. The flight-like siderostat consists of a 380 mm light-weighted flat mirror with an embedded cube corner at the center. The siderostat is located inside a thermal shroud that simulates the on-orbit flight-like thermal environment.

The on-orbit thermal disturbance is mainly from the change in the relative position of the sun with respect to SIM. The typical SIM observation scenario will generate about 7 degrees of spacecraft motion every hour in order to slowly cover the entire sky. A relatively smaller thermal disturbance is from the change in the position of the siderostat relative to the rest of the instrument hardware due to the articulation of the siderostat. The siderostat will acquire light from stars anywhere in the 15 degrees field of regard. These two sources of thermal disturbances are emulated in TOM3 using the thermal shroud.

2. COMMON-PATH HETERODYNE INTERFEROMETER

The COPHI uses standard heterodyne metrology techniques, but it has been modified in order to do precise relative metrology of various portions of the pupil. Details on the COPHI can be found in references ^{7,8}. Figure 3 illustrates the COPHI metrology in the vacuum chamber as well as the laser source outside of the vacuum chamber.

The coherent laser light from a 532 nm frequency-double Nd:YAG laser is split into two beams that we will be named in the rest of the paper "Local Oscillator" (LO) and "Measurement Beam" (MB). The frequency of these two laser beams is then shifted by respectively 80 and 80.01 MHz using acousto-opto-modulators (AOMs). Using a pair of single mode polarization-maintaining fibers designed for 532nm, the laser light is brought to the COPHI sub-bench in the vacuum chamber.

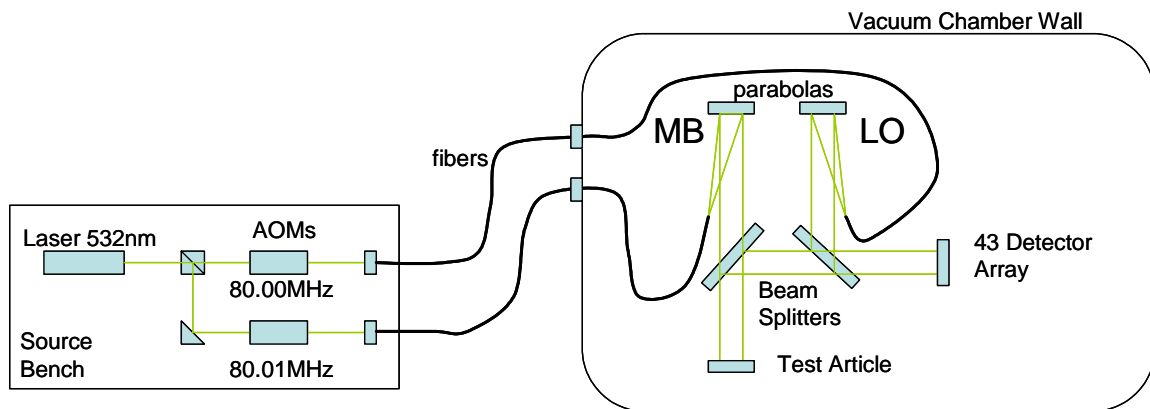


Figure 3. COPHI detection

The light from the two fibers is collimated using off-axis parabolas. A pair of 50/50 beam splitter windows forms the main interferometer. Each of the beam splitters has a specific role. The measurement beam transmits through the first beam splitter window, propagates to the test article, retro-reflects and returns back to the same beam splitter. The light that reflects from that beam splitter window propagates to the second beam splitter window where it mixes and interferes with the local oscillator beam. Additional paths and reflections do not contribute to the metrology and are not displayed in Figure 3. In order to maintain required stability within the interferometer, the two parabolas and beam splitters are mounted on top of a Zerodur glass bench, which has a very low coefficient of thermal expansion.

The combined light is then collected by an array of 43 photo-detectors. The detectors are sampled in the pupil plane as shown in Figure 4. A 10 kHz sine wave signal, due to the interference of the 80 MHz MB signal with the 80.01 MHz LO signal, is observed at each detector. In a perfect optical system, all detectors would produce 10 kHz sine waves in phase. In the real case, the aberration in the optical wavefront at the beam recombination produces relative phase offsets between the 10 kHz waves at the various detectors. This relative phase difference is measured very accurately by the COPHI phase-meter electronics, providing a precise measurement of the aberration in the wavefront (or OPD change).

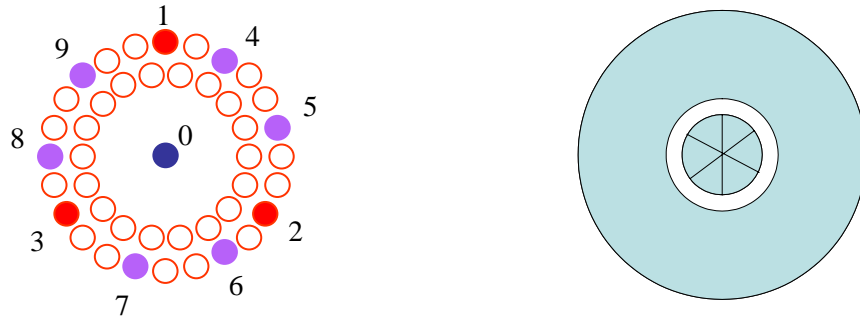


Figure 4. Location of the 43 COPHI detectors (Left Figure) in respect with the siderostat pupil plane (Right Figure). To reduce the size of the COPHI electronics, the 43 signals are multiplexed. Ten detectors can be recorded at a time, of which 4 are fixed and read continuously (detector 0 at the center of the array and detectors 1, 2 and 3 in the outside at 120 degrees from each others) and 6 are selectable using the multiplexer.

A custom VME phase-meter board⁹ produces the precise relative phase measurement at every zero crossing of the 10kHz signal. The relative phase detection uses a fast counter at 128MHz that starts on the reference signal and stops on the target signal. We have chosen to always use the signal produced by the central detector (in Figure 4) as the reference. The single measurement resolution[†] of the phase meter at 10kHz is approximately 40pm. However, the phase meter is capable of on-board averaging to obtain a much finer resolution. Sub-picometer resolution can be achieved after a few seconds of integration.

The test article under measurement with COPHI is one of the three following optics:

- A small 75mm diameter reference flat mirror, located right next to the COPHI optics, used for calibration of the COPHI.
- The large 500mm diameter chopping/fold reference flat mirror, located in the expanded beam side of the compressor, used to monitor the thermal performance of the flight-like beam compressor.
- The flight-like 380mm diameter siderostat flat mirror, with an embedded cube-corner at its center, located in the expanded beam side of the compressor.

Finally, using the light from the other port of the main recombination beam splitter in the COPHI sub-bench, the pupil is imaged on a CCD camera (Figure 2) in order to achieve good system alignment prior to the start of each test. By setting the heterodyne frequency to a very low rate (about 1 Hz), the pupil camera can be used to estimate the static wavefront error, achieving a resolution similar to the Zygo phase shifting interferometers¹⁰.

3. TEST ARTICLES

3.1. Flight-like beam compressor

SIM's optical beam compressor assembly is designed to receive optical starlight reflected from the siderostat. The compressor is a three-mirror anastigmat telescope design, with a flat fold mirror to make it compact. This light is compressed by a ratio of 7:1 (from 35cm entrance beam to a 5cm exit beam). The optical path is shown in Figure 5.

[†] The instantaneous resolution of the phasemeter can be calculated from the ratio of the fast clock to the heterodyne frequency and from the metrology laser wavelength:

$$532\text{nm} * 10\text{kHz} / 128\text{MHz} = 0.041\text{nm} \sim 40\text{picometers.}$$

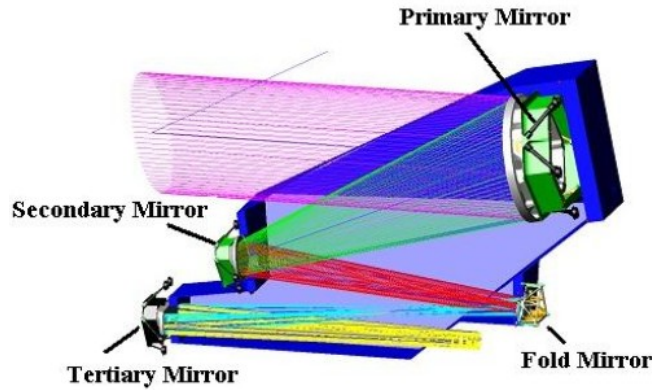


Figure 5. Beam compressor optical path

The flight-like compressor tested in TOM3 consists of a large composite optical bench, built by ATK, which constrains four static mirror assemblies: the primary mirror, secondary mirror, fold mirror, and tertiary mirror. The composite panels form an egg-crate structure. The light-weighted mirrors, polished by Tinsley, were aligned by SSG Precision Optronics, Inc. Table 1 lists the major components of the assembly.

Table 1. Flight-like compressor hardware list

Component	Function	Material
Compressor Bench	Low CTE metering support of the optics	Carbon composite
M1 Mirror Glass	Receives 350mm diameter optical beam	ULE
M1 Mirror Mount	Supports M1 mirror glass	Invar
M2 Mirror Glass	Receives optical beam from M1	ULE
M2 Mirror Mount	Supports M2 mirror glass	Invar
Fold Mirror Glass	Receives optical beam from M2	ULE
Fold Mirror Mount	Supports Fold mirror glass	Invar
M3 Mirror Glass	Receives optical beam from Fold mirror	ULE
M3 Mirror Mount	Supports M3 mirror glass	Invar

The compressor bench was not located within the thermal shroud and was instead passively thermally controlled with Multi-Layer Insulator (MLI) blankets. The lack of thermal control made the bench susceptible to diurnal temperature changes in the chamber wall as well as soak changes from the presence of the cold liquid nitrogen shroud in the chamber. However, the resulting thermal environment turned out to be very similar to the expected beam compressor on-orbit thermal environment.

3.2. Flight-like siderostat

The primary test article is the flight-like siderostat shown in Figure 6. The siderostat optic consists of a 380 mm light-weighted ULE-glass flat mirror, built by Tinsley, with an embedded Zerodur-glass Double Cube Corner (DCC) at the center, built by Research Electro-Optics, Inc. Table 2 lists the major components of the assembly.

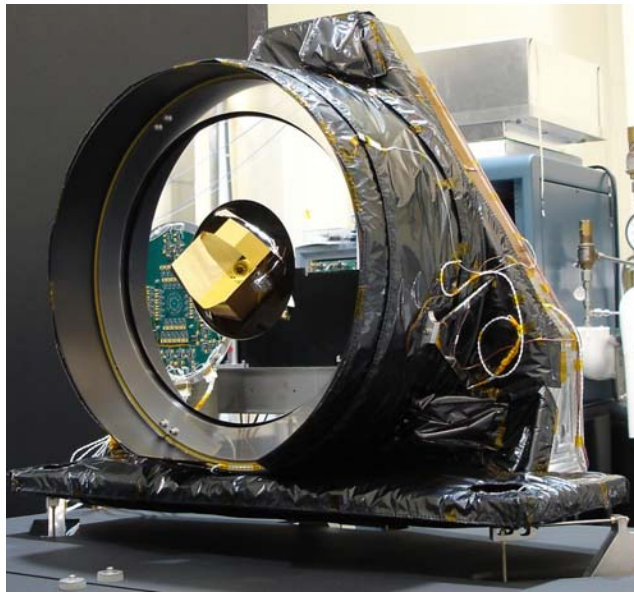


Figure 6. Flight-like siderostat

The siderostat optic is thermally controlled by an aft thermal can (radiative enclosure surrounding the mirror). A forward thermal can extends beyond the plane of the mirror face in order to reduce mirror lateral thermal gradients. Platinum Resistance Thermometers (PRT) on the aft thermal can control seven heater patches wired in parallel. Heaters are driven by a Lakeshore 332 controller using a Proportional-Integral-Derivative (PID) heater control. Details of heater properties and their locations are shown in the next section.

Table 2. Flight-like siderostat hardware list

Component	Function	Material
Siderostat Flat Mirror	380mm diameter reflecting surface	ULE glass
Bezel	Supports siderostat mirror	Super Invar
De-Space Monopods	Contains PZT actuators for alignment	Invar
De-Center Monopods	Holds bezel to support structure	Invar
Support Structure	Supports mirror assembly	Invar
Double Corner Cube	Sampled by SIM's metrology	Zerodur glass
DCC Post	Supports DCC	ULE glass
Aft Thermal Can	Mirror radiative thermal control	Aluminum
Forward Thermal Can	Reduces lateral thermal gradients	Aluminum
Thermal Can Bipods	Supports thermal can from structure	Titanium
Interface Bipods	Supports entire assembly from bench	Invar

Fine pointing of the siderostat is achieved with three PZT actuators connecting the siderostat support structure with the siderostat bezel. Coarse pointing actuation of the siderostat was not implemented for the TOM3 test. This omission is the primary difference between the TOM3 siderostat and the flight design. Instead of using a coarse pointing actuator, the temperature field of the thermal enclosure is varied to simulate the changing thermal environment around the siderostat.

The siderostat support structure consists of two large Invar parts. The vertical part of the support fixture is controlled by a PID heater circuit consisting of 5 heater patches. The horizontal part of the support fixture is controlled by a PID heater circuit consisting of one heater patch. The entire mirror assembly is supported from the optical bench on three bipods with bases machined from invar and bipod legs made from stainless threaded rod. The bipods also provide thermal isolation for the siderostat.

The siderostat assembly is located inside the thermal shroud described in the next section. The shroud simulates flight-like boundary temperatures (190K to 250K) for the siderostat. The inside walls of the shroud assembly are actively controlled to ensure very stable boundary conditions.

4. THERMAL SYSTEM

4.1. Vacuum chamber

The TOM3 testbed is installed inside a 3.3 meter vacuum chamber at the Jet Propulsion Laboratory. The chamber is equipped with a turbo molecular pump as well as a cryogenic getter plate for high vacuum. For thermal testing, it is important to have a high vacuum, as the thermal conduction through the remaining gas (mostly nitrogen) in the chamber at 10^{-4} Torr pressures is high enough to add significant heat leak to the siderostat. This makes thermal model correlations much more difficult. During the TOM3 test, we maintained the vacuum chamber pressure near 10^{-6} Torr level.

The 3.3x2.1 meter optical table is supported on air isolators, located outside the chamber, with thin-wall bellows feed-through to the platforms that contact the table. After fine adjustment, they provide mechanical isolation of the optical bench from the tank and the thermal shroud in six degrees of freedom. Additionally, all of the connections to the chamber required vibration isolation measures.

4.2. Thermal shroud

The thermal shroud has a box configuration and consists of a dual panel construction (Figure 7). The goal of this construction was to provide a stable boundary temperature for the siderostat by attenuating any temperature fluctuations on the liquid nitrogen (LN₂) panels by utilizing the thermal capacitance of the plates as well as the radiative heat exchange between the plates. Both sets of panels are 6mm thick and are painted with Aeroglaze Z-306 black paint. The outer shroud panels are cooled by LN₂ supply lines, vacuum brazed to the outer side. During the test, these lines are kept flooded to ensure as stable temperatures as possible.

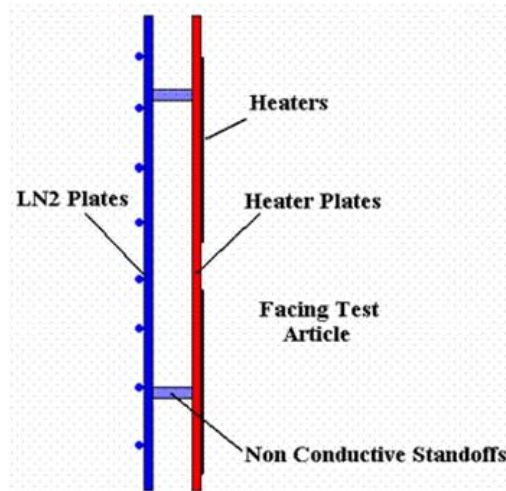


Figure 7. Shroud dual panel construction

The interior panels are actively temperature controlled with Lakeshore PID temperature controllers to the desired set-points. All of the panels are controlled on separate heater circuits so different set-points could be used in for each. Film heaters, providing at least 80% coverage for an even heat flux, are mounted to the interior panels facing the inter-panel space. Very stable temperatures (± 10 mK/hr) were achieved on the inner heater panels while the outer LN₂ panels were flooded with LN₂. Five of the six inner panels are conductively isolated from the outer panels by means of G-10 standoffs. The door inner panel however, is conductively coupled to the outer door panel by aluminum standoffs to simulate the open aperture boundary condition of a flight-like Collector Bay.

The thermal shroud can be operated to provide both steady state and transient conditions. The LN₂ panels are flooded at all times to provide a constant heat sink. Transient temperature changes on the heater plates are induced to simulate the changes in temperature of the internal Collector Bay MLI during nominal spacecraft slew and siderostat mirror articulation in space. The transient temperature profiles are based on thermal models of the spacecraft in a flight-like environment.

4.3. Thermal sensors

For areas where changes in temperature need to be accurately measured, Platinum Resistance Thermometers (PRT) sensors with individual calibration curves are used, providing a resolution of approximately ± 3 mK. Thermocouples are used where the precision and expense of PRT are not warranted. TDAS (Thermal Data Acquisition System), a JPL developed LabView based data acquisition system is used for this test. All data (time, date, temperature, power, voltage, and current) are monitored and automatically recorded at one-minute intervals.

5. MODELING ISSUES FOR HIGH PRECISION

Though the stability requirements for SIM appear daunting, the thermo/opto/mechanical modeling for the TOM3 testbed was done with commercial, off-the-shelf tools that were integrated via a “bucket brigade” process. In the bucket brigade, each of the discipline analyses was applied sequentially, with the output of one modeling tool used to supply the input to the next tool.

Although the ultimate precision of the OPD changes that must be modeled is very high, the physical and temporal scales of the system make it amenable to the application of conventional methods. The picometer precision is measured on large, massive systems (relative to pm) over long times (30 s to 1 h) so that the atomic-level thermal and quantum fluctuations that are sometimes brought up as a concern are averaged out and can be ignored. Additionally, the data optical data are post-processed to remove some types of common mode or systematic errors.

Because classical physics can be used, the physical phenomena involved are well understood: the thermal transport is largely radiation with some contribution from conduction, the structural deformations are caused by temperature-induced strains and are well within the small deformation range of continuum mechanics, the optical effects are well described by geometric optics for computation of the OPD.

Mechanical design was done in I-deas¹¹. Temperature predictions were made using TMG¹² and transferred directly into an I-deas structural deformation model in order to calculate the resulting mirror wave-front error or OPD. This OPD prediction was then transferred over to an Optics model in CODE-V¹³ to predict optical performance. For the most critical temperatures, the siderostat mirror, DCC, and DCC post, the same finite element mesh was used in both the structural and thermal models so that there would be no interpolation error.

The extremely high precision required accurate geometry modeling. This involved aspects of using the correct design models, capturing all significant components, and enveloping the component volumes in elements with significant completeness. In addition to capturing the component volumes, the thermal analyst needed to accurately capture the radiation view factors.

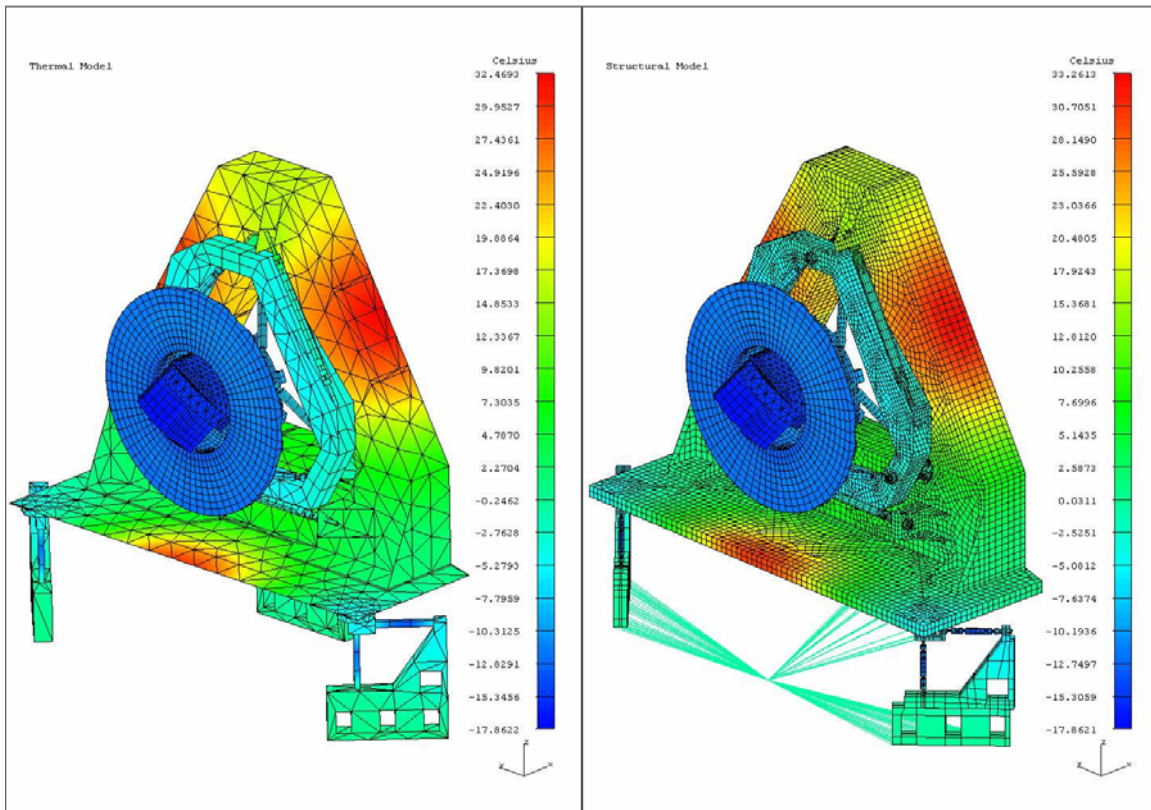


Figure 8. Example FEM mapping of thermal (Left Figure) and structural (Right Figure) models for the siderostat.

5.1. Material properties

Material properties were among the largest sources of uncertainty in the TOM3 modeling process. Common materials, such as aluminum and steel are fairly well understood but were not suitable for the SIM optical systems. Primary material properties of interest for the TOM3 modeling are Coefficient of Thermal Expansion (CTE), Young's modulus (E) and Poisson's ratio. Temperatures create strain via CTE. All three properties appear linearly in structural equations. Young's Modulus E varies +/- 5% across lots, although values are not tabulated in Mil-HDBK-5¹⁴.

Athermal materials such as ULE, Zerodur, Invar, which were used in the SIM hardware, are often "tuned" for particular characteristics at in a specified environment. For example, the coefficient of thermal expansion for ULE glass may be 0+-20 ppb at a specified temperature, but there can also be significant inhomogeneities within a single large sample, as well as temperature dependence when used at temperatures away from the design point. Zerodur has also been reported to show hysteresis that could potentially complicate modeling and analysis. The models described here used constant values for the material properties, with no time or temperature dependence.

5.2. Time dependence

Time dependence in the modeled systems was addressed through transient thermal models, which were then used to drive the structural models. The thermal changes in the system occur slowly enough that the thermally induced structural deformations can be treated as quasi-static, and addressed simply by solving the structural model at various times of interest using snapshots from the transient thermal model as inputs.

The thermal problems in TOM3 and those currently being used for system design are slowly time varying, modeling maneuvers of several hours duration. The flight hardware under test, primarily the siderostat but also the compressor, are very well designed thermally. The primary thermal energy transport mechanism from the environment to the test articles is radiation and it far exceeds that transported by conduction. As a result, the fundamental time constants of the hardware (~10 hrs) are still short compared to the driving temperature change rates (~24 hrs).

5.3. Numerical precision

One potential issue in the modeling of large systems, such as the SIM collector system, to such high precision is the possibility of the numerical methods themselves becoming a limitation on the quality of the modeling. These effects can appear as a result of roundoff or truncation errors that propagate into the more significant digits of the results during computations with many iterations, or they can be a function of the internal precision of the computer or software package.

The thermal problem is non-linear because of the T^4 term and must be solved in absolute temperatures, and is thus of concern, since we are working in mK around 293 K. The possibility of this causing difficulty was recognized early, and efforts were made to identify any possible issues. The manufacturer of TMG¹² went through their code to verify how calculations were done, and provided the modelers with details of where single and double precision numbers were used, and how. The temperature problem is solved in double precision and the results are preserved until conversion to relative temperatures in single precision for the structural problem. Additionally, models were run under a variety of conditions and no signs of instability or unusual behavior of the tools was observed.

The structural problem is less of an issue because it is linear and is solved in relative temperatures. For a temperature time series, the driving structural temperatures for each step are relative to the first step. This reduces the required dynamic range of the model and relieves the pressure on floating point precision.

5.4. Compressor model

Although it was not located in the thermal shroud the compressor was in a very stable thermal environment. In addition to the isolation of the vacuum chamber, it was also covered with MLI blankets and additional MLI blankets limited the view factor from the open side of the compressor to the chamber walls. The outside of the thermal shroud was also blanketed, preventing the compressor from seeing the cold LN2 shroud directly. The typical temperature variations of the compressor were +/-1 K/day, with a 24 hour period. Thermal models of the flight system show that this is comparable in both rate of change and magnitude to the temperature variations expected during normal operation in space.

Because the compressor was not in as tightly controlled a thermal environment, a simple 1 K thermal soak (uniform temperature change) was modeled and the effects were calculated using the structural FEM and the Code V optical model. Only this one case was needed because all models use time and temperature independent material properties and larger temperature changes can be simply scaled from the 1 K case.

The FEM for the compressor bench was delivered by ATK, who also manufactured the compressor bench. The model has approximately 200,000 nodes and 250,000 elements. Details on modeling the composite laminate material and Invar fittings can be found in reference¹⁵. All mirrors and their mounts inside the compressor bench, were modeled at JPL, with

approximately 100,000 nodes and 50,000 elements per optic. In order to provide results for the compressor, the mirror FEMs had to be integrated with the compressor bench model from ATK.

5.5. Siderostat model

The siderostat thermal model shared direct associativity with CAD geometry in the TeamCenter CAD database. This ensured that the thermal, structures, and optical models would all be based off of one solid model representation and that all hardware representations in the models would occupy the same positions in space. The right handed picture of Figure 8 shows the FEM developed for the siderostat. This model has 47,000 elements and 168,000 nodes.

6. TEST RESULTS

6.1. Beam compressor OPD

Figure 9 shows data from a TOM3 test run, characterizing the compressor thermal response. COPHI metrology data (left plot) was recorded simultaneously with thermal data (right plot) for almost 50 hours. The optical metric of interest is the OPD between the central detector and the average of nine detectors, uniformly located in the outer ring, after reflection from the large reference flat on the expanded beam side of the beam compressor. The five thermal sensors were mounted on the beam compressor, three on the composite bench, one on the primary mirror glass and the last one on the secondary mirror glass. One can observe a static thermal gradient within the compressor and a soak temperature change.

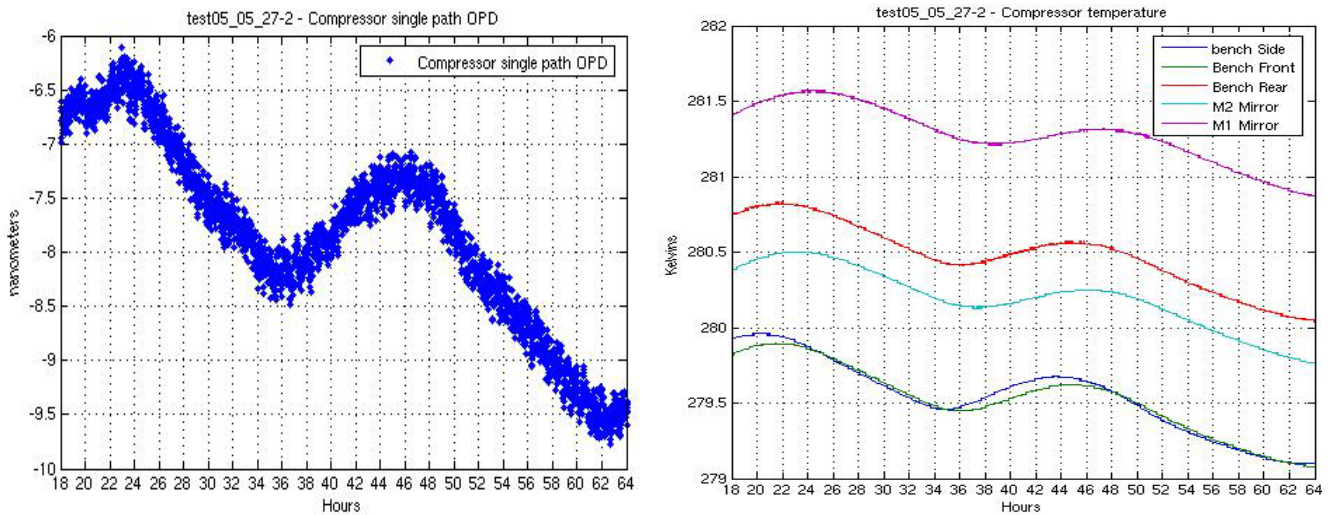


Figure 9. COPHI metrology data (Left Plot) in nanometers and temperatures (Right Plot) in Kelvins from the beam compressor.

Comparing the optical data and the thermal data from Figure 9, one can see an obvious correlation between the thermal excitation and the optical response. The slow downward drift and the diurnal cycle of the temperature suggest a 4 nanometers per Kelvin linear thermo-opto-mechanical sensitivity of the compressor (single path).

In comparing the compressor model output to the experimental data, it was particularly important to ensure that the model accurately followed the experimental setup. Simply taking the average or RMS deviation of the surface would produce misleading results, as the mirror mounts provide a non-uniformity to the deformation of the surface, and the detectors only sample particular points on the surface. When the proper position and alignment was used, the predicted single path OPD change was 4.98 nm/K, as compared to the 4 nm/K measured value.

6.2. Guide interferometer prediction

SIM's guide interferometer collecting optics consists only of a beam compressor on each arm of the interferometer. This is simulated on TOM3 when the chopping mirror is in the retro-mode position. Using data from runs similar to the run presented in the previous section, one can estimate the Guide interferometer performance by processing the data as it would be done on the flight system.

In SIM's wide angle observation scenario⁵, the linear drift of the instrument is estimated and removed every hour, by repeating the same observation at the beginning and the end of the hour. Within each hour, the data is integrated for 30 seconds at a time to mimic the integration on SIM's target stars. In SIM's narrow angle observation scenario⁴, twelve chops between a target and a reference stars are averaged together. The 30 second integration time and the 90 second chop period help in reducing the sensitivity to fast noise (faster than a few seconds) as well as very slow fluctuations (slower than a few

milli-Hertz) and drift of the instrument. The first two rows in Table 3 show the final post-processed results for the Guide interferometers: 99 pm wide angle and 5.4 picometers narrow angle.

6.3. Beam compressor wavefront

The left picture of Figure 10 shows a sample frame from the pupil camera showing interference fringes from the light reflected on the beam compressor with the local oscillator light. Tilt was applied to put a number of fringes across the pupil, however, in normal operation, the tilt is removed. The distortion of the fringes is due to the aberration on the compressor wavefront. The right picture of Figure 10 shows the wavefront phase map processed from a series[‡] of 360 frames from the pupil camera. The relatively large distortion (390 nm PV) does not meet the wavefront quality requirement of the flight compressor. The source of this wavefront error was linked to an inappropriate support fixture use during testing of the primary mirror of the compressor. Time constraints of the TOM3 experiment did not allow us to re-polish the primary mirror to meet the flight requirement.

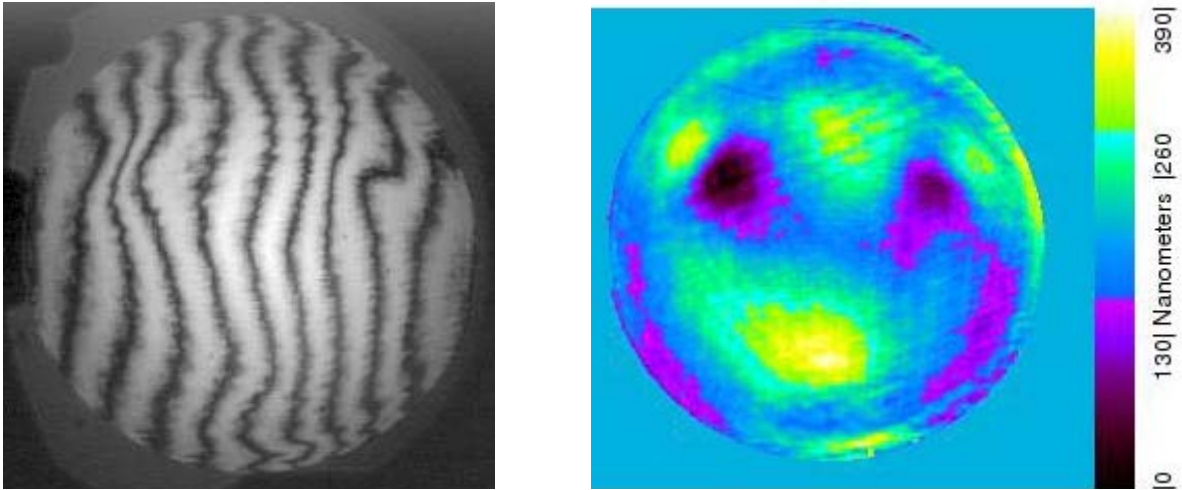


Figure 10. Left picture: sample frame from the pupil camera showing the distorted fringes due to the aberration on the compressor wavefront. Right picture: post-processed phase map of the compressor wavefront.

The left picture in Figure 11 shows a differential wavefront surface map of the beam compressor measured in TOM3 after a 8.4 K temperature drop. The right picture of Figure 11 shows the analytical results due to an increase of 1 K in soak temperature of the beam compressor primary optics. A visual analysis demonstrates an excellent correlation between the measured values and the analytical results. The RMS value for the tested article is 25.5 nm and a P-V of 240 nm. This translates to an RMS of 6.1 nm/K OPD error and a P-V of 14.25 nm/K surface error. The analytical results were calculated as RMS OPD error 7.2 nm/K OPD and a P-V surface error of 14 nm/K.

[‡] The 360 frames used to generate the phase map scan about 30 waves.

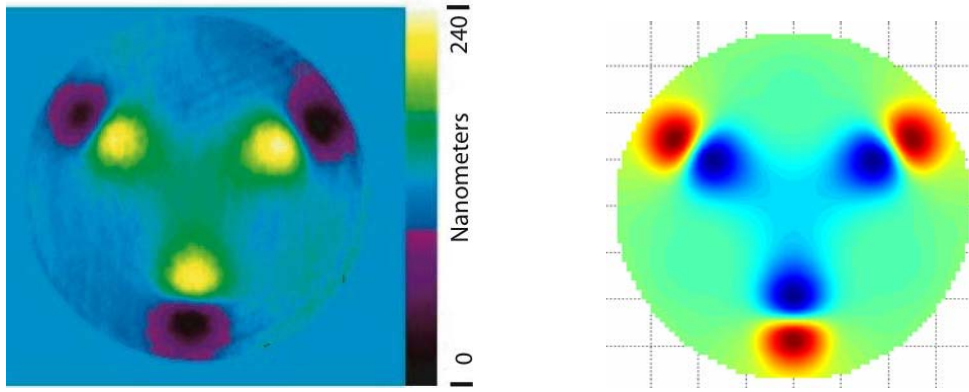


Figure 11. Difference in measured phase map of the beam compressor compared to predicted deformation map from the structural model. Left picture: measured distortion after a uniform temperature drop of 8.4 K. Right picture: predicted distortion for a uniform temperature increase of 1 K. The peaks and valleys correspond to the mirror mount interface.

6.4. Science interferometer

SIM's science interferometer collecting optics consists of a siderostat followed by a beam compressor on each arm of the interferometer. This is simulated on TOM3 when the chopping mirror is in the siderostat position.

The left-hand picture of Figure 12 shows the temperatures measured inside the thermal shroud during a typical TOM3 test run. The shroud panel temperatures range from 95 K at the door panel that simulates cold space to 210 K at the top panel that simulates the MLI temperature of the instrument panel on the sunny side of the spacecraft. The siderostat and DCC temperatures are kept near ground room temperature (290 K) by the PID thermal control.

The right-handed picture of Figure 12 shows more details on the temperature measured on the thermal shroud side panels during the same test run. The one-hour-period variation of the temperature simulates the change in the thermal load on the siderostat as it would articulate to acquire stars in the sky. The slower 14-hour-period variation of the temperature simulates the change in the thermal load on the siderostat due to the spacecraft motion.

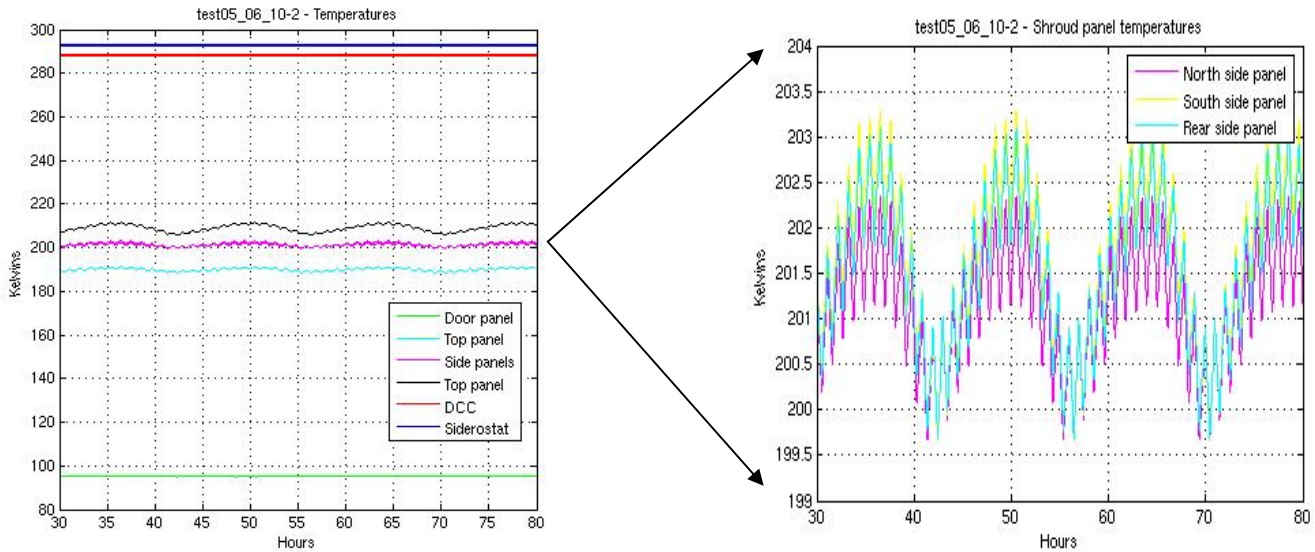


Figure 12. Left plot: temperatures of the siderostat mirror, double corner-cube and shroud panels during a typical 50 hour run.

Right plot: shroud temperature during the siderostat test. The Top panel temperature at 190 K, the Bottom panel temperature at 210 K and the Door panel at 95 K are not visible at this scale.

Figure 13 shows the temperature variation of the siderostat mirror surface and DCC. Although the shroud temperature is around 200 K, the mirror surface is kept at the required 293 K thanks to the siderostat thermal control. The DCC is more exposed to the shroud thermal load than the siderostat, so its temperature is about 5 K cooler. The one-hour-period thermal excitation is not observable on the siderostat article optics. The 14-hour-period thermal excitation is significantly attenuated by the siderostat thermal control scheme, from about 2 K amplitude (in Figure 12) down to 50 mK at the siderostat surface and 25 mK at the DCC.

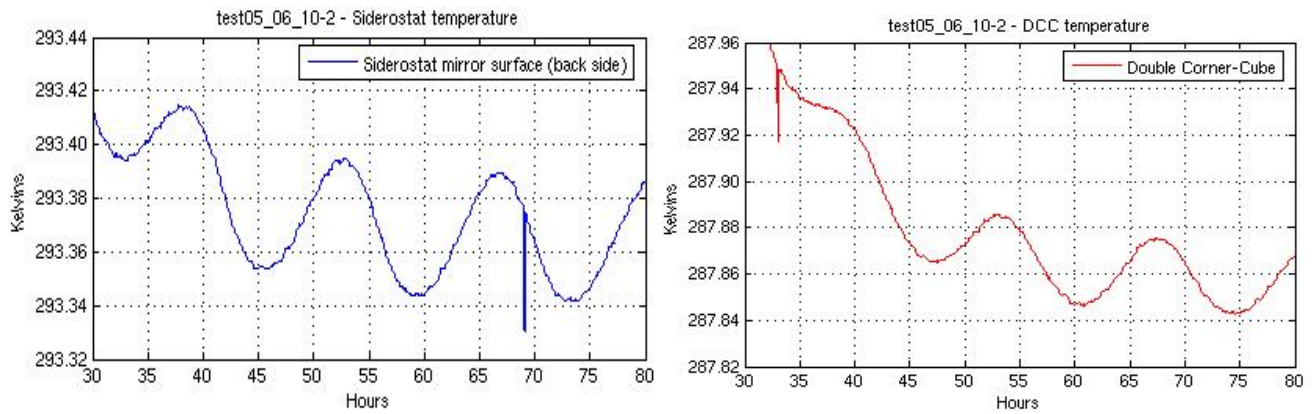


Figure 13. Temperature variations on the siderostat (left plot) and double corner-cube (right plot) during the siderostat test.

Figure 14 shows the raw COPHI metrology data that was recorded continuously at 10Hz for about 50 hours. The metric of interest is the optical path difference between the central detector that samples the cube corner at the center of the siderostat optic and the average of nine detectors, uniformly located in the outer ring, after reflection from the mirror portion of the siderostat. The constant value (around 60 nanometers) in the data, due to the residual defocus aberration of the beam compressor (one tenth of a wave at 633 nm) was removed. Note a slow downward drift mostly produced by the diurnal cycle of the temperature outside of the vacuum chamber. Slow fluctuations of a few 100 picometers over several hours were traced back to thermal instability of the optical fibers that bring the laser light into the chamber.

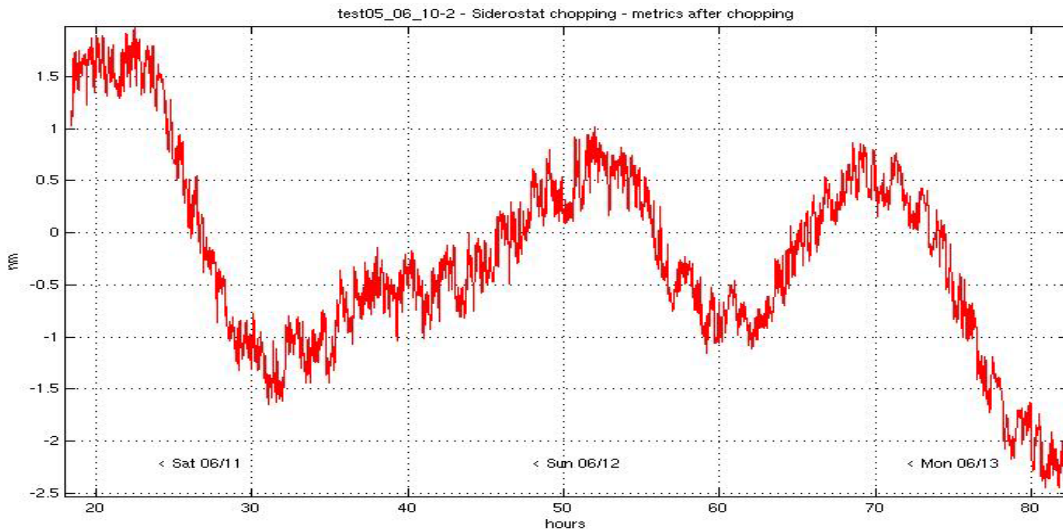


Figure 14. COPHI measurement of the siderostat optical path difference of the average of 9 detectors relative to the central detector, in nanometers.

The last four rows in Table 3 show the final post-processed results for the Science interferometers. In the Science interferometer tests, both the beam compressor and the siderostat are tested. Also, during the science test, the temperature in the thermal shroud is varied in a flight-like manner to simulate either the Inboard collector bay at about 200K or the Outboard bay at about 190K.

6.5. Siderostat OPD

Figures 16 show the predicted OPD variations with time for two the test runs, along with empirical data. OPD predictions were made in three different ways: fully modeled, in which thermal model predictions were made and put into the structural model to generate OPD outputs; partially modeled, in which an empirical value of OPD as a function of siderostat temperature was measured and simply multiplied by the temperatures from the thermal model; and empirically modeled, in which the previously measured $dOPD/dT$ number was simply multiplied by the measured temperature changes.

These results suggest that detailed knowledge of CTE values is very important in developing accurate models for the siderostat. The partially modeled and fully empirical predictions use the temperature difference between the DCC and the siderostat mirror, which crosses the boundary between two different materials, Zerodur and ULE. Both materials have very

low CTE whose sign can be + or -, and which can vary from sample to sample of the material. Additionally, the CTE of ULE is inhomogeneous, and due to constraints in manufacturing neither the particular Zerodur nor ULE sample used in the siderostat are well characterized. Despite this, the models show that OPD changes can be predicted a priori to within about a factor of 2, which is acceptable for these components of SIM. Careful characterization during manufacture or testing at intermediate stages of fabrication might improve this predictive capability at reasonable expense. Further, the close correlation of the OPD to the temperature difference from the DCC to the siderostat might offer the capability of further reducing thermally induced errors in the completed system, even if they can't be perfectly predicted prior to assembly.

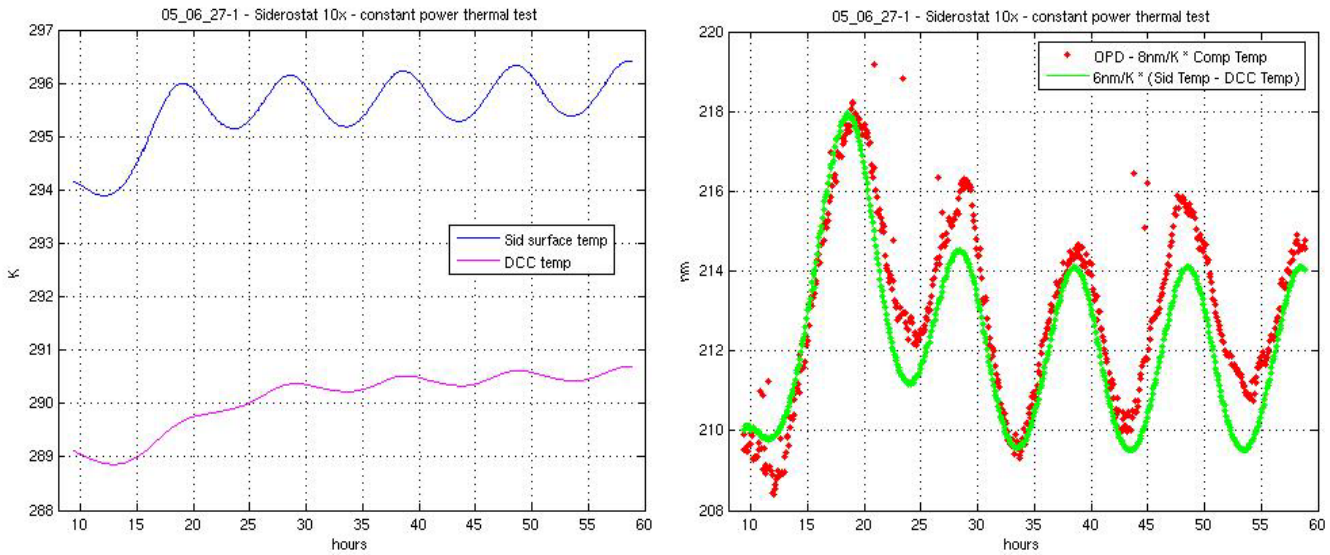


Figure 16. Siderostat Optical Path Difference data and empirical model fit.

6.6. Performance summary

Table 3 summarizes about 500 hours of thermal testing on the TOM3 testbed. The results are sorted by type of test. In the Guide interferometer tests, only the beam compressor is tested. In the Science interferometer tests, both the beam compressor and the siderostat are tested. Also, during the science test, the temperature in the thermal shroud is varied in a flight-like manner to simulate either the Inboard collector bay at about 200K or the Outboard bay at about 190K.

Table 3. TOM3 test summary

Test	Baseline Requirement	Run Time	Test Result
Guide Narrow Angle - Either Bay	10.8 pm	108 hours	5.4 pm
Guide Wide Angle - Either Bay	280 pm	148 hours	99 pm
Science Narrow Angle - Inboard Bay	22.2 pm	56 hours	9.5 pm
Science Wide Angle - Inboard Bay	570 pm	40 hours	198 pm
Science Narrow Angle - Outboard Bay	22.2 pm	56 hours	8.7 pm
Science Wide Angle- Outboard Bay	570 pm	85 hours	204 pm

The baseline requirement allocated from SIM's error budget is shown in the first column. Note that the tests meet all the requirements with some margin. SIM is also carrying a goal performance budget, about 4 times tighter than baseline error budget. The test results do not meet that goal performance. However, further testing showed that the current TOM3 performance is limited by the stability of the optical fibers that inject the light in the COPHI interferometer. Thermally "overdrive" tests confirmed that the test article thermal performance is significantly better than the results indicate.

7. CONCLUSION

We have discussed the TOM3 testbed developed to assess the thermo-opto-mechanical stability of optical assembly such as SIM's siderostat and telescope in flight-like thermal conditions. Although limited by the metrology sensor noise, test results

show that optical wavefront stability of SIM's optical assembly is compatible with single micro-arcsecond astrometry. Comparisons of test results with model predictions show that the integrated modeling process is working and allows thermo/opto/mechanical modeling at levels needed for SIM. The process takes advantage of commercially available FEA tools without need for additional tool development.

The thermal models using the best available inputs predicted the relevant parameters (peak-to-valley temperature change and rate of change) to within 60% prior to any attempts to adjust model parameters to fit the experimental data. For most components of interest, except for the DCC, the model over-predicted the temperature swings and rate of change. After relatively small adjustments that are physically reasonable, the model consistently matches the experimental results or over-predicts by 20 to 60%. Over-prediction is preferable to under-prediction because it provides margin against design or modeling errors.

The structural models are fairly sensitive to accurate knowledge of material parameters, particularly CTE, but also provided performance predictions that are valuable for flight development. Prior to model correlation, the structural model of the siderostat under-predicted by a factor of 3. After modifying the CTE of the ULE glass in the model to be more consistent with the properties of the real glass, including inhomogeneity, the model under-predicted by a factor of about 1.6. Although over-prediction would be preferred, this very reasonable and also gives us a modeling uncertainty factor that is useful for developing design margins for the flight system that aren't prohibitively conservative.

These data, combined with an empirical model of the siderostat system also suggest that a combination of more detailed knowledge of material properties, possibly combined with tests at the component and subsystem level, can improve the fidelity of the models for use in design modifications or for integration into higher level models.

8. ACKNOWLEDGEMENTS

The research described in this publication was performed at the Jet Propulsion Laboratory of the California Institute of Technology, under contract with the National Aeronautics and Space Administration.

9. REFERENCES

1. J. C. Marr IV, "SIM-Planet Quest progress report", SPIE Conference on Advances in Stellar Interferometry, vol. 6268, 2006.
2. R. A. Laskin, "Successful completion of SIM-Planet Quest technology", SPIE Conference on Advances in Stellar Interferometry, vol. 6268, 2006.
3. R. Goullioud, O.S. Alvarez-Salazar, and B. Nemat, "Dim star fringe stabilization demonstration using pathlength feed-forward on the SIM Testbed 3 (STB3)", SPIE Conference on Interferometry in Space, vol. 4852, 2002.
4. R. Goullioud and T. J. Shen, "SIM astrometric demonstration at 24 Picometers on the MAM Testbed", IEEE Aerospace Conference, Big Sky, MT, 2004.
5. R. Goullioud, T. J. Shen, and J. H. Catanzarite, "Wide angle astrometric demonstration on the Micro-Arcsecond Metrology testbed for the Space Interferometry Mission", International Conference on Space Optics, Toulouse, France, 2004.
6. F. G. Dekens, "Kite: status of the external metrology testbed for SIM", SPIE Conference on New Frontiers in Stellar Interferometry, vol. 5491, 2004.
7. F. Zhao, J.E. Logan, S. Shaklan, and M. Shao, "A common-path, multi-channel heterodyne laser interferometer for sub-nanometer surface metrology", SPIE International Conference on Optical Engineering for Sensing and Nanotechnology, vol. 3740, pp. 642-645, 1999.
8. F. Zhao, "Demonstration of sub-Angstrom cyclic non-linearity using wavefront-division sampling with a commonpath laser heterodyne interferometer", American Society for Precision Engineering annual meeting, Crystal city, VA, 2001.
9. P. Halverson, D. R. Johnson, A. Kuhnert, S. B. Shaklan, and R. E. Spero, "A multi-channel averaging phase meter for picometer precision laser metrology", SPIE International Conference on Optical Engineering for Sensing and Nanotechnology, vol. 3740, 1999.
10. Zygo Corporation, Laurel Brook Road, Middlefield, CT 06455, USA. Also <http://www.zygo.com>
11. UGS Corporation, 5800 Granite Parkway, Suite 600, Plano, TX 75024, USA. Also <http://www.ugs.com>.

12. Maya Heat Transfer Technologies Ltd, 4999 St. Catherine St. West, Suite 400, Montréal, Quebec, Canada, H3Z 1T3. Also <http://www.mayahtt.com>
13. Optical Research Associates, 3280 East Foothill Boulevard, Suite 300, Pasadena, California 91107, USA. Also <http://www.opticalres.com>
14. Mil HDBK-5, Metallic Materials and Elements for Aerospace Vehicles and Structures, US Department of Defense, 2001.
15. C. A. Lindensmith, H. C. Briggs, Y. Beregovski, V. A. Feria, R. Goullioud, Y. Gursel, I. Hahn, G. Kinsella, M. Orzewalla, C. Phillips, "Development and validation of high precision thermal, mechanical, and optical models for the Space Interferometry Mission", *IEEE Aerospace Conference*, Big Sky, MT, 2006.